JOURNAL OF MATERIALS SCIENCE **34** (1999) 251–256

Structure and properties of new perovskites La_2MRhO_6 (M = Mg, Zn)

C. SCHINZER
Institut de Chimie de la Matière Condensée de Bordeaux, (E.N.S.C.P.B.), (I.C.M.C.B. UPR-CNRS 9048), 87, Avenue du Docteur A. Schweitzer, F-33608 Pessac cédex, France

G. DEMAZEAU
Interface Hautes Pressions, Avenue Pey-Berland, BP. 108, F-33402 Talence cedex, France

New perovskite type oxides of Rh(IV) (La_2MRhO_6; M = Mg, Zn) have been prepared by conventional techniques used in solid state chemistry. Rietveld refinements from X-ray diffraction data confirm the space group $P2_1/n$ for both compounds. This low symmetry is a result of two effects: (i) slight $GdFeO_3$-type distorsion of the ideal perovskite structure due to the size of six-fold co-ordinated B cations and (ii) 1/1 ordering of the B-cations. The observed lattice parameters are $a = 0.557\,9(1)$ nm, $b = 0.561\,5(1)$ nm, $c = 0.789\,8(1)$ nm, $\beta = 90.01(6)^\circ$ for La_2MgRhO_6 and $a = 0.558\,4(3)$ nm, $b = 0.565\,9(3)$ nm, $c = 0.791\,4(4)$ nm, $\beta = 90.0(2)^\circ$ for La_2ZnRhO_6, respectively. The magnetic moment localized on Rh(IV) is strongly reduced compared to the spin-only value. The reasons for this phenomenon are discussed accounting for theoretical work on the magnetic behaviour of $^2T_{2g}$-terms. However, a weak antiferromagnetic exchange interaction is observed. Both materials are intrinsic semiconductors.

1. Introduction

Many mixed metal oxides of perovskite-type containing a 3d element in a high oxidation state, such as Fe(IV), Fe(V), Co(IV), Ni(III) etc., have been prepared and studied [1]. The strong increase of the local crystal field energy (10 Dq) from 3d to 4d and then 5d elements generally improves the stabilization of the high valencies. In the group Co–Rh–Ir, the highest value is +IV for Co and +VI for Ir, but in the case of Rh +IV appears to be the limit.

The objective of this work was primarily the preparation and study of Rh(IV) oxides with perovskite structure, where the Rh(IV) cations are isolated from each other.

2. Experimental procedure

2.1. Preparation

La_2MgRhO_6 and La_2ZnRhO_6 compounds have been synthesized from $La(NO_3)_3 \cdot 6H_2O$ (Prolabo, 99.99%), $Rh_2O_3 \cdot 5H_2O$ (Johnson Matthey, 99.9%) and $Mg(NO_3)_2 \cdot 6H_2O$ (Aldrich, 99%) or $Zn(NO_3)_2 \cdot 6H_2O$ (Prolabo, 99%), respectively, by mixing the appropriate stoichiometric ratio together. Initial grinding was then followed by thermal decomposition of the nitrates at about 500 °C.

Thereafter the resulting materials were calcined in an oxygen flux at 800 °C (96 h), 1000 °C (48 h) and 1100 °C (24 h) with intermediate grindings in an agate mortar. The reaction was followed by X-ray diffraction.

2.2. Analysis

The oxygen content of the samples has been determined by iodometric titration following the method of Bunsen. The sample is treated for 30 min in boiling HBr.

Elementary bromine is formed due to the reduction of Rh and is then distilled into a KI solution. Then, we determine the resulting iodine concentration by titration using 0.1 N–$Na_2S_2O_3$ solution and the starch–iodine indicator complex to find the end-point of the titration.

Energy dispursive X-ray (EDX) microanalyses were performed on a Cameca FX 100.

2.3. X-ray diffraction

X-ray diffractograms for Rietveld analysis were taken on a Philips PW 3040/00 X'pert MPD system. K_α radiation from a ceramic Cu tube operated at 40 kV50 mA has been used in a Bragg–Brentano set-up equipped with an analyser crystal (PG). For Rietveld refinement, the FullProf 3.1 software package [2] was used. Definitions of R_p, R_{wp}, R_{exp} and R_{Bragg} are given in the corresponding manual.

2.4. Magnetic and conductivity measurements

Magnetization of the compounds was measured on a Quantum Design SQUID magnetometer in a magnetic flux of 1 kG. The molar susceptibility, χ_{mol}, was calculated from the measured magnetization and corrected for atomic diamagnetic contributions, given by Selwood [3]. All units concerning the magnetic behaviour are given in the cgs-emu system.

TABLE I Results of chemical analysis for La_2MRhO_6

	EDX microanalysis								
	La ($\%_{atom}$)		B ($\%_{atom}$)		Rh ($\%_{atom}$)		O ($\%_{atom}$)		Iodometry
M	Found	Calculated	Found	Calculated	Found	Calculated	Found	Calculated	Ox(Rh)
Mg	20.9(5)	20	10.1(7)	10	9.2(3)	10	59.8(2)	60	+4.00(2)
Zn	20.7(6)	20	10.5(9)	10	9.0(9)	10	59.7(4)	60	+3.97(2)

The electric conductivity of the samples was measured using an automated sampling system, using a Keithley 220 current source and a Keithley 181 nanovoltmeter. Pellets of about 1 mm thickness were pressed from the powder samples for this purpose and recalcined for 4 h at 1100 °C under an oxygen flux.

3. Results

3.1. Oxidation states and microanalysis

The results from EDX microanalysis and iodometric titration are summarized in Table I. The oxidation state of rhodium was found to be +IV in both samples. Microanalysis confirmed the expected atomic ratio between the elements in the samples, i.e. the stoichiometries found were La_2MgRhO_6 and La_2ZnRhO_6, respectively.

3.2. Crystal structure and Rietveld refinements

The X-ray diffractogram of La_2MgRhO_6 shows a single phase whose reflections were in a first approach completely indexable in a cubic unit cell with $a = 0.790\,9(3)$ nm. That of La_2ZnRhO_6, however, contains a small fraction of an unknown impurity. The perovskite phase is also indexable in a cubic unit cell of $a = 0.793\,8(8)$ nm. In both XRDs, systematic extinctions, corresponding to an F-centred unit cell are not observed, but any cubic superstructure of perovskite type would show these. In a more detailed analysis of the diffractograms, an orthorhombic unit cell with $a \approx b \approx \sqrt{2} \times a_P$ and $c \approx 2 \times a_P$ could be attributed to both diffractograms. Still, the special extinction rules for the $GdFeO_3$ unit cell were not met in this indexing, but should occur, if the Rh- and M-cations were randomly distributed on the B-positions [4]. Cation ordering in the $GdFeO_3$-type structure is known for several $La_2BB'O_6$ mixed oxides [5, 6], and leads to a monoclinic space group with a monoclinic angle β very close to 90°. The axes are re-named accounting for the related symmetry elements, thus we have $a \approx c \approx \sqrt{2} \times a_P$ and $b \approx 2 \times a_P$.

In order to confirm the cation ordering, we performed a profile matching run in space group *Pnma* (No. 62; disordered $GdFeO_3$-type) and in space group $P2_1/n$ (No. 14; the ordered variant) before considering the structure factors. The *R*-values obtained by these refinements are very close to each other (cf. Table II). Obviously, the only difference between the two crystallographic set-ups consists of the cation ordering.

TABLE II R-values of Rietveld refinements for La_2MRhO_6

	Pnma (No. 62)			$P\,2_1/n$ (No. 12)		
M	R_p (%)	R_{wp} (%)	R_{exp} (%)	R_p (%)	R_{wp} (%)	R_{exp} (%)
Profile matching						
Mg	10.2	13.5	7.79	8.91	11.7	7.75
Zn	13.8	22.5	4.27	13.7	24.1	4.68
Rietveld refinement[a]						
Mg	15.0	20.5	7.91	10.4	13.6	8.01
Zn	17.4	27.0	4.87	14.7	22.9	4.96

[a]Cf. Tables III and IV for crystallographic and atomic parameters.

TABLE III Rietveld refinement results for La_2MgRhO_6[a,b]

Atom	Site	*x*	*y*	*z*	Occ.
La	4e	0.511(1)	0.5391(7)	0.250(3)	1.0(——)
Mg	2d	0.5	0	0	1.0(——)
Rh	2c	0	0.5	0	1.0(——)
O(1)	4e	0.215	0.2154	−0.045	1.0(——)
O(2)	4e	0.295	0.703	−0.041	1.0(——)
O(3)	4e	0.4213	−0.0175	0.249	1.0(——)

[a]$a = 0.557\,9(1)$ nm, $b = 0.561\,5(1)$ nm, $c = 0.789\,8(1)$ nm, $\beta = 90.01(6)°$.
[b]$R_p = 10.4\%$, $R_{wp} = 13.6\%$, $R_{exp} = 8.01\%$, $R_{Bragg} = 3.12\%$.

TABLE IV Rietveld refinement results for La_2ZnRhO_6[a,b]

Atom	Site	*x*	*y*	*z*	Occ.
La	4e	0.512(3)	0.545(2)	0.249(4)	1.0(——)
Zn	2d	0.5	0	0	1.0(——)
Rh	2c	0	0.5	0	1.0(——)
O(1)	4e	0.203	0.213	−0.0481	1.0(——)
O(2)	4e	0.295	0.697	−0.0395	1.0(——)
O(3)	4e	0.4118	−0.0208	0.251	1.0(——)

[a]$a = 0.558\,4(3)$ nm, $b = 0.565\,9(3)$ nm, $c = 0.791\,4(4)$ nm, $\beta = 90.0(2)°$.
[b]$R_p = 14.7\%$, $R_{wp} = 22.9\%$, $R_{exp} = 4.96\%$, $R_{Bragg} = 8.48\%$.

Rietveld refinements have thus been performed in both space groups and resulted in the *R*-values given in the lower part of Table II and confirm monoclinic cation-ordered space groups for both compounds. The results of the refinement are given in Tables III and IV for La_2MgRhO_6 and La_2ZnRhO_6, respectively. The graphic results of the refinements are represented in Figs 1 and 2.

Both structures have been refined from the starting values given for La_2MgIrO_6 and La_2ZnIrO_6 by Battle and Gore [7], leaving the oxygen parameters untouched during the whole refinement. The isotropic temperature factors of the metal ions could not be refined, since they lead to negative values; thus, the overall temperature

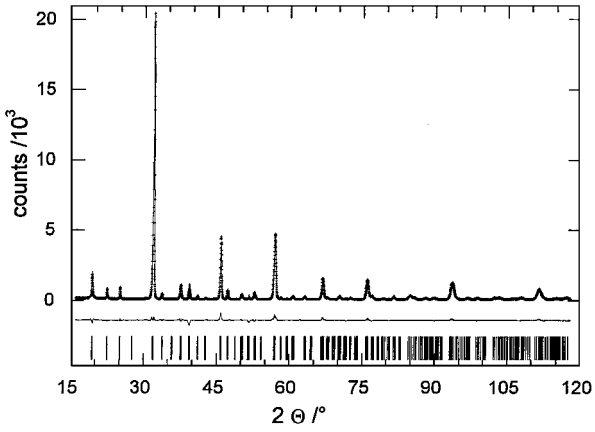

Figure 1 Final plot of the Rietveld refinement for La_2MgRhO_6.

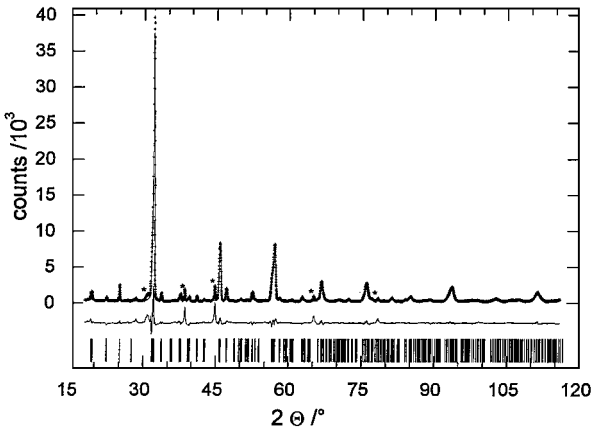

Figure 2 Final plot of the Rietveld refinement for La_2ZnRhO_6 (stars denote an unidentified impurity phase).

factor has been fixed at 0.003 nm^2, which corresponds to the values reported for the Ir-analogues [7].

Negative temperature factors generally indicate an absorption effect, but we were not able to correct for microabsorption applying the corrections given by Pitschke *et al.* [8]. Consequently, the site occupancy factors were not refinable, too, and have therefore been fixed to the ideal values. Both compounds show best results in the monoclinic space group, thus confirming at least an important fraction of cationic order on the B-positions.

3.3. Magnetic properties

The molar magnetic susceptibilities, χ_{mol}, and the corresponding effective magnetic moment, μ^2_{eff}, curves are shown in Fig. 3. Both perovskites exhibit paramagnetic behaviour. Since rhodium is an element of the second row of the transition elements, it is expected that the

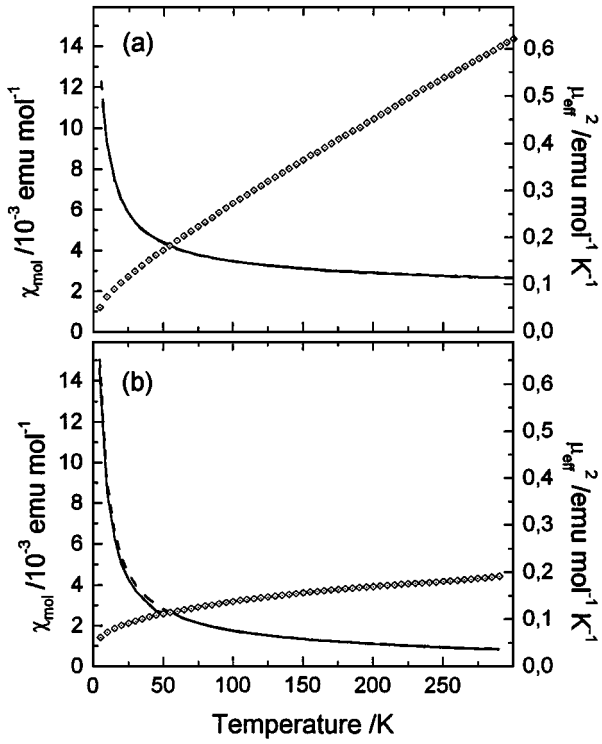

Figure 3 Molar magnetic susceptibility (left scale; lines) and square effective magnetic moment (right scale; symbols) for La_2MgRhO_6 (a) and La_2ZnRhO_6 (b).

electronic configuration of Rh(IV) corresponds to a $4d^5$ low spin system (t^5_{2g}; term $^2T_{2g}$). Assuming localized electrons, a spin-only value of 1.73 Bohr magnetons (BM) is calculated.

Usually, the effective magnetic moment, μ_{eff}, of T-terms is a function of temperature, though $1/\chi_{mol}$ versus T is not expected to be linear. Nevertheless, the susceptibility curves could be parameterized applying a modified Curie–Weiss law, with an additional temperature-independent susceptibility. Note that, given our X-ray diffraction results, we exclude temperature-independent paramagnetism arising from band electrons.

The parameters determined by applying the modified Curie–Weiss law are summarized in Table V. The μ^2_{eff} found for the linearized part of the $1/\chi_{mol}$ versus T curve corresponds to 1.142(3) and 1.184(3) BM for La_2MgRhO_6 and La_2ZnRhO_6, respectively.

Moreover, our fit to the $1/\chi_{mol}$ versus T curve results in slightly negative Curie constants, Θ. This suggests weak antiferromagnetic interactions in both compounds, that can also be seen in the slope of the μ^2_{eff} versus T curves. At very low temperatures, both curves drop towards zero.

TABLE V Results of fits to magnetic and conductivity data on La_2MRhO_6

	Magnetic parameters				Conductivity	
M	C (emu K^{-1} mol^{-1})	Θ (K)	χ_{tip}[a] (cm^3 mol^{-1})	μ_{eff} (BM)	$\sigma_{300\,K}$ (mS)	E_A (kJ mol^{-1})
Mg	0.163(1)	−21(1)	0.0021(1)	1.142(3)	15.2(5)	4.1(3)
Zn	0.174 5(9)	−17.3(7)	0.000 25(3)	1.184(3)	4.53(5)	4.9(5)

[a]Temperature-independant contribution to molar susceptibility as fitted.

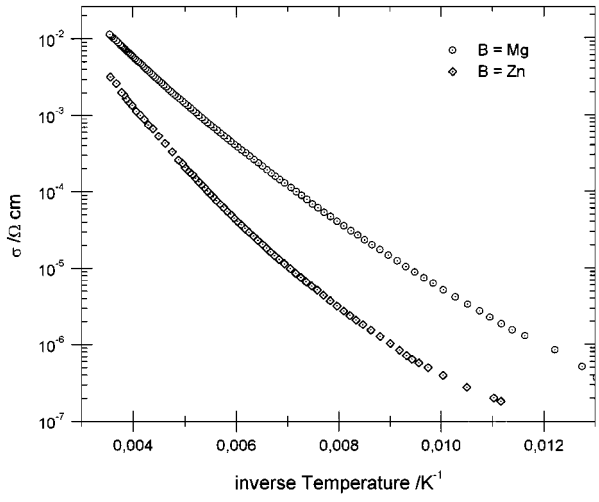

Figure 4 Specific electrical conductivity of La_2BRhO_6 as a function of inverse temperature.

3.4. Electric conductivity

The specific electric conductivity of the compounds is presented in Fig. 4 in an Arrhenius plot. A semiconducting behaviour is found for La_2MgRhO_6 as well as for La_2ZnRhO_6. The characteristics of electric conductivity are presented together with the magnetic parameters in Table V.

Both, the specific conductivity, σ, at room temperature and the activation energy, E_A, determined from the Arrhenius plot indicate, that La_2MgRhO_6 is a better electric conductor than La_2ZnRhO_6. In both cases, the Arrhenius plot does not result in a pure, linear slope. In the case of extrinsic semiconductors obeying a hoping-conduction mechanism, the slope can often be modelled by a modified Arrhenius law accounting for the dimensionality, D, of the conduction mechanism [9, 10]. Such an attempt led to $D > 3$ in our case, which is not a reasonable value.

By fitting the ordinary Arrhenius law to our data we determine $E_A = 4.1(3)$ kJ mol^{-1} [0.042(3) eV] for La_2MgRhO_6 and $E_A = 4.9(5)$ kJ mol^{-1} [0.050(5) eV] for La_2ZnRhO_6.

4. Discussion

4.1. Crystal structure

An ordered structure is induced both by the size difference and the charge difference between the two B-cations. In our case, the difference in charge is fair and the cationic radii do not differ largely (in octahedral co-ordination Mg(II) and Zn(II) are 1.20 and 1.23 times the size of Rh(IV) if we account for the radii given by Shannon [11]). Nevertheless similar cationic ordering is observed for La_2BIrO_6 perovskites [6, 7], where B represents Mg, Co, Ni, Cu and Zn. This is noteworthy, since Ir(IV) (0.066 nm [11]) is bigger in size than Rh(IV) and the size difference of the B-cations is therefore even less in those perovskites, thus the tendency to obey an ordered structure should be decreased. We attribute the observation of ordered perovskites to the fact that the covalency of the M–O bond rises with the element number and is important for the second- and third-row transition metals; though the driving force for ordering may be assigned to a chemical effect more than to the physical effect of size difference.

As stated above, both diffraction profiles could be completely indexed in cubic cells of about 0.8 nm. This observation can be explained by the relatively low crystallite size of both samples that lead to rather broad peaks. A close inspection of the shape of the peaks at high diffraction angles reveals their mutiple nature. Nevertheless, distortion of the ideal cubic perovskite structure is very small. This is not surprising, since the Goldschmidt factor, τ, is near the ideal value of one for both compounds ($\tau = 0.95$ and $\tau = 0.94$ for M = Mg and Zn, respectively).

The observed cation ordering is confirmed by our magnetic and electric measurements. In the case of a disordered structure we expect either a stronger influence of the magnetic interactions between neighbouring Rh(IV) cations [12, 13] or the formation of Rh-rich clusters leading to largely increased electric conductivity [14]. None of these observations are made, thus we take this as confirmation of our cation-ordered structure model.

4.2. Magnetic properties and electronic structure

Compared to the spin-only value given for low-spin Rh(IV), we detect a clearly reduced magnetic moment for both compounds, even at room temperature. One may argue, that Rh-electrons are delocalized into bands and that this is the reason why we observe a temperature-independent paramagnetic contribution. Considering the Rh/M ordering, such a delocalization could be induced by the overlap of the t_{2g}-orbitals of Rh along the face diagonal of the perovskite cell. Such a behaviour is not observed for the higher homologue La_2ZnIrO_6, where expansion of the t_{2g} orbitals is larger, thus we cannot consider this hypothesis to be true for the Rh(IV) perovskites. We must, moreover, bear in mind, that band formation in perovskites containing low-spin d^5 ions will usually lead to metallic behaviour. Although this extreme is inhibited by the second B-cation in our case, we do not even find strongly enhanced conductivity, but semiconducting properties with rather high activation energies. La_2ZnIrO_6 shows semiconducting behaviour, with even higher activation energy, too [6]. In the light of these results we can exclude collective effects and consequently the delocalization of electrons into bands.

For fully localized electrons we will have to consider the rules set up by Goodenough [12] and Kanamori [13] in order to determine the type of super-super-exchange [15] interaction between two Rh(IV) centres. The results are summarized in Table VI. The super-super-exchange between two Rh(IV) centres is a weak but nevertheless present interaction. The pathway of this interaction is shown in Fig. 5. We deduce from Table VI, that the probability of finding antiferromagnetic interaction between two half-filled Rh-t_{2g} orbital is 1/9, whereas a half-filled ferromagnetic interaction with a full t_{2g} orbital is found in 4/9 of the cases. The

TABLE VI Expected Rh(IV) super-super-exchange interactions in La_2MRhO_6

Site 1		Site 2		Result[a]
e_g	Empty	e_g	Empty	—
1 t_{2g}	Half	1 t_{2g}	Half	AF
2 t_{2g}	Full	2 t_{2g}	Full	FM
		1 t_{2g}	Half	FM
		2 t_{2g}	Full	—

[a]FM, ferromagnetic; AF, antiferromagnetic.

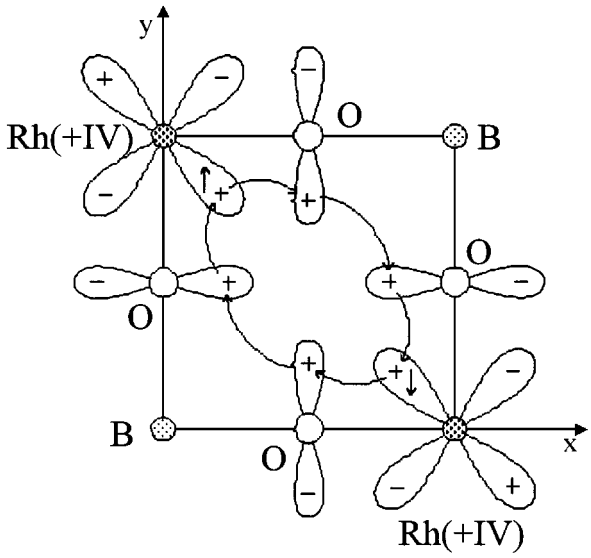

Figure 5 Model of the super-super-exchange mechanism in perovskites (adapted from Buffat *et al*. [15]).

remaining combinations of all-full t_{2g} orbitals do not comprise a magnetic interaction.

In a model of localized electrons on Rh(IV), spin–orbit coupling plays an important role, as is generally the case for 4d and 5d metal ions. According to Kotani's theory [16], the effective magnetic moment of the Rh(IV) ion should be raised to values superior to the spin-only value due to spin–orbit coupling effects. However, μ_{eff} is a function of $kT/|\lambda|$, where λ represents the spin–orbit coupling constant. Our results imply a nearly linear dependence of μ^2_{eff} on T, we do not observe an enhanced magnetic moment in the case of La_2MgRhO_6 and La_2ZnRhO_6. As indicated by Figgis [17], two other effects affect the magnetic behaviour of T-terms. These are (i) perturbation of the ideal octahedral co-ordination and (ii) transfer of electrons into the metal–ligand bond. The first affects the shape of the μ^2_{eff} versus T curve, whereas the second generally decreases the value of μ^2_{eff}. Both effects shall be discussed in more detail below.

Local perturbation of the octahedral crystal field can be obtained by two different mechanisms, one being the influence of the "crystallographic" change of the co-ordination symmetry, the other being induced by the electronic configuration of the centre ion. A study of single crystals in the series $RFeO_3$ (R = rare earth) [18], where Fe(III) is an "ideal" centre ion with no tendency to perturb the octahedral crystal field, showed that deformation of the B–O-octahedra in $GdFeO_3$-type oxides is small, even in cases where distortion of the ideal perovskite structure by octahedra tilting is important. Local perturbation of the crystal field symmetry can also be induced by the electronic ground state of the centre ion, as stated above. Because of its anisotropic electronic configuration (LS $4d^5$) Rh(IV) is a Jahn–Teller ion. The Jahn–Teller effect of Rh(IV) will probably have a tendency to stabilize the two filled t_{2g}-orbitals against the half-filled one. If the effect is strong enough, the electronic ground state will consequently no longer be a T-, but an A-term. Such a distortion will moreover enhance the antiferromagnetic exchange interaction of the two half-filled orbitals of higher energy.

We do not expect quenching of the magnetic moment due to charge transfer from the oxygen ligands. A similar effect has been found for compounds containing trivalent copper ($NaCuO_2$, $La_2Li_{0.5}Cu_{0.5}O_4$), where X-ray absorption spectroscopy studies revealed a strong donor-effect of the oxygen ligands, such that the Cu(III) centres were "reduced" to Cu(II) [19]. At the same time the magnetic moment of the whole complex is invariant, because the spin-orientation of the donated electron remains unchanged.

When we take into account the inductive effect of the next metal neighbours Mg(II) and Zn(II) in the Rh–O–M chain, both enhance the donor-effect on the Rh-side, but Zn(II) probably less than Mg(II). The effective moments found by the Curie–Weiss approach do not reflect this situation significantly, though the electronic nature of the B cations does not severely affect the character of the Rh–O bond in our case. A recent iridium-Mössbauer study on the ordered compounds $A_2MIr(VI)O_6$ has shown that the isomer shift seems to be independent of the ionicity of the competing bond [20].

The fact that we do not observe ordering in the investigated temperature range is due to the weakness of the super-super-exchange effect. The strength of the exchange interaction is enhanced by two factors: (i) decreasing bond distance and (ii) increasing covalency of metal–oxygen bonds. We shall take the super-super-exchange of Fe(V) in La_2LiFeO_6 as an example. In this compound, the ordering temperature is around 10 K and the Fe–O bond distance is 0.186 nm [21]. The mean Rh–O distance in our compounds is 0.201 nm, though we would expect a far lower ordering temperature. On the other hand, the covalency of the metal–oxygen bond usually rises when we go from 3d to 4d and 5d metals. We illustrate the influence of this effect using Ba_2CaIrO_6 as an example, where the reported Néel temperature is 55 K [22]. Nevertheless it must be stressed that Ir is hexavalent in this example and the covalency is higher for 5d elements, thus the super-super-exchange is strongly enhanced in that compound.

Conclusively, we believe that the effective magnetic moment in La_2MgRhO_6 and La_2ZnRhO_6 is reduced by antiferromagnetic interaction of the Rh(IV) centres via the super-super-exchange mechanism.

Acknowledgements

C.S. holds a TMR Marie-Curie Research Training Grant of the European Union (Contract No. ERB

FMB ICT 961859). We acknowledge the assistance of E. Marquestaut (electric measurements), E. Lebraud (XRD) and H. Montigaud (microanalysis).

References

1. G. DEMAZEAU, in "High Pressure Chemical Synthesis", edited by J. Jurczk and B. Baranowski (Elsevier, Amsterdam, 1989) Ch. 5.
2. J. R. CARVAJAL, *FullProf*, Version 3.1 for Macintosh^{TM} PPC (1997).
3. P. W. SELWOOD, "Magnetochemistry", 2nd edn (Interscience, New York, 1956).
4. S. GELLER, *J. Chem. Phys.* **24** (1956) 1236.
5. G. BLASSE, *J. Inorg. Nucl. Chem.* **27** (1965) 993.
6. E. M. RAMOS, I. ALVAREZ, M. L. VEIGA and C. PICO, *Mater. Res. Bull.* **8** (1994) 881.
7. P. D. BATTLE and J. G. GORE, *J. Mater. Chem.* **6** (1996) 1375.
8. W. PITSCHKE, N. MATTERN and H. HERMANN, *Powder Diffraction* **8** (1993) 74 and 223.
9. N. MOTT, "Conduction in Non-crystalline Materials" (Clarendon Press, Oxford, 1976) p. 27.
10. B. I. SHKLOVSKII and A. L. EFROS, "Electronic Properties of Doped Semiconductors", Springer Series in Solid-State Sciences, Vol. **45** (Springer Verlag, Berlin, 1984) p. 203.
11. R. D. SHANNON, *Acta Crystallogr.* **A32** (1976) 751.
12. J. B. GOODENOUGH, *Phys. Chem. Solids* **6** (1958) 287.
13. J. KANAMORI, *ibid.* **10** (1959) 87.
14. J. B. GOODENOUGH, *Phys. Rev.* **171** (1968) 466.
15. B. BUFFAT, G. DEMAZEAU, M. POUCHARD, J. M. DANCE and P. HAGENMULLER, *J. Solid State Chem.* **50** (1983) 33.
16. M. KOTANI, *Jpn. J. Appl. Phys.* **4** (1949) 293.
17. B. N. FIGGIS, *Trans. Faraday Soc.* **57** (1961) 198.
18. M. MAREZIO, J. P. REMEIKA and P. D. DERNIER, *Acta Crystallogr.* **B26** (1970) 2008.
19. A. BIANCONI, J. BUDNICK, G. DEMAZEAU, A. M. FLANK, A. FONTAINIE, P. LAGARDE, J. JEGOUDEZ, A. REVCOLEVSKI, A. MARCELLI and M. VERDAGUER, *Physica C* **153–155** (1988) 117.
20. D.-Y. JUNG, PhD thesis, Université Bordeaux I (1995).
21. J. L. SOUBEYROUX, B. BUFFAT, N. CHEVREAU and G. DEMAZEAU, *Physica B* **120** (1983) 227.
22. G. DEMAZEAU, D.-Y. JUNG, J.-P. SANCHEZ, E. COLINEAU, A. BLAISE and L. FOURNES, *Solid State Commun.* **85** (1993) 479.

Received 1 June
and accepted 4 August 1998